

## Evaluation of radiation environment at FRIB linac

Mikhail Kostin<sup>1</sup>, Robert Lowrie<sup>1,2</sup>, Reginald Ronningen<sup>1</sup>

<sup>1</sup>Facility for Rare Isotope Beams, US

<sup>2</sup>URS Corporation, US

### Abstract

*The Facility for Rare Isotope Beams (FRIB) at Michigan State University is a project jointly funded by the US Department of Energy and Michigan State University with the construction started in March 2014. This accelerator facility will use a broad range of primary ion beams from <sup>16</sup>O to <sup>238</sup>U with a beam power of up to 400 kW and energy of 200 MeV/nucleon for <sup>238</sup>U in its baseline configuration to produce rare isotopes. A possible facility upgrade will include increase of the beam energy up to 400 MeV/nucleon for <sup>238</sup>U and the addition of new light ion beams down to <sup>3</sup>He and protons for ISOL operations.*

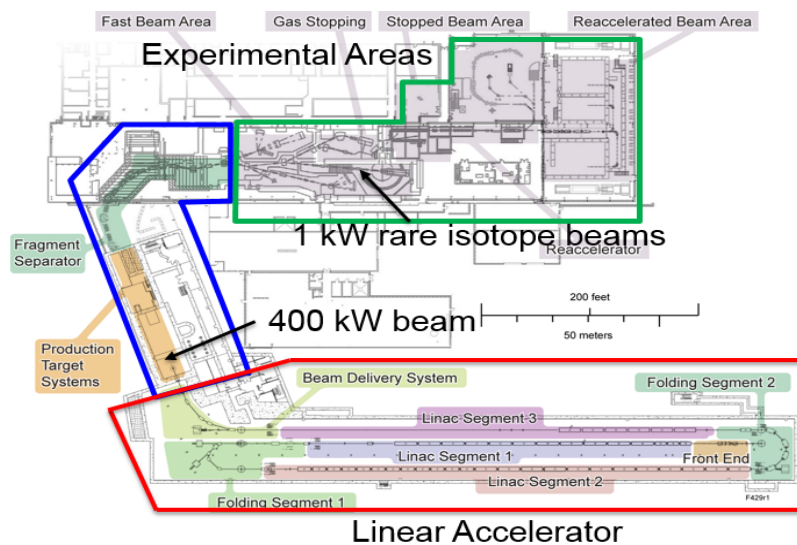
*The work presented here is an overview of radiation transport calculations aimed to evaluate the radiological environment at the FRIB linac and adjacent areas. A number of calculations have addressed the impact on environment (activation of soil and ground water, evaluation of radionuclide releases); prompt radiation to the workers and general public due to normal beam losses and beam loss incidents; and activation of services.*

*This material is based on work supported by the US Department of Energy Office of Science under Cooperative Agreement DE-SC0000661.*

### Introduction

The Facility for Rare Isotope Beams (FRIB) is a new national user facility at Michigan State University (MSU). The facility is being built for the research in the fields of physics of nuclei, nuclear astrophysics, fundamental interactions, and applications for society. In its baseline configuration the facility will offer separation of isotopes in-flight for fast, stopped and reaccelerated secondary beams. A broad range of the primary ion beams will be utilised, from <sup>16</sup>O to <sup>238</sup>U with a beam power of up to 400 kW and energy of 200 MeV/nucleon for <sup>238</sup>U (higher for lighter primary beams) to produce rare isotopes. A possible facility upgrade will include an increase in the primary beam energy up to 400 MeV/nucleon for <sup>238</sup>U and the addition of new light ion beams down to <sup>3</sup>He and protons for Isotope-Online (ISOL) operations. A multi-user operation with simultaneous light and heavy primary beams is also considered.

FRIB will consist of two major systems: a double-folded linear accelerator which will deliver a primary ion beam to a rare isotope production facility, consisting of a high-power target connected to a fragment separator for providing secondary rare isotope beams for science experiments (see Figure 1). This paper provides an overview of the radiation transport calculations performed in support of the design of the FRIB linear accelerator and its radiation shielding with focus on human and environmental impact issues rather than on the design of specific beam line elements.

**Figure 1. Schematics of the FRIB Facility and the experimental areas**

### Regulatory protection criteria applied to FRIB

One of the goals of the radiation transport calculations is to provide input to the designers to verify that the facility meets the limits from various regulatory agencies and satisfy the MSU ALARA (As Low As Reasonably Achievable) goals both for the general public and the radiation workers. One key factor for this analysis is that FRIB is situated on the MSU campus where the general public is immediately outside the facility walls and not in a remote location. Although FRIB is largely funded by the US Department of Energy, the regulatory agencies include the US Nuclear Regulatory Commission (NRC), whose limits are the applicable regulations for this study. FRIB will be under an independent NRC license. Table 1 summarises various limits. The MSU ALARA goals are in general set to 10% of the limits imposed by the regulatory agencies. One distinctive difference is the self-imposed limits for the ground water activation. The limits for effluent water shown in Table 1 show the significant margin being applied to the design by using the drinking water limits. Groundwater near FRIB is not in contact with any source of drinking water nor public access. FRIB is relatively distant from the closest drinking water well and the aquifer is relatively deep under FRIB. Nonetheless, the design goal is to assure radiation protection for the ground water activation level by meeting the limits established for the drinking water.

**Table 1. Regulatory radiation protection limits and MSU ALARA goals**

Type of limit	Limits and goals	
Radiation dose – Worker	Standard [1]: 5,000 mrem/yr MSU ALARA Goal [2]: 500 mrem/yr	
Radiation dose – Public	Standard [1]: 100 mrem/yr and < 2 mrem/(any one hour) MSU ALARA Goal [2]: 10 mrem/yr and < 2 mrem/(any one hour)	
Air – maximum exposure to nearest receptor	Standard [1]: 10 mrem/y MSU ALARA Goal [2]: 1 mrem/yr	
Groundwater - effluent	<sup>3</sup> H Standard [1]: 1,000 pCi/ml FRIB Design Goal: 20 pCi/ml (drinking water standard [3])	<sup>22</sup> Na Standard [1]: 6 pCi/ml FRIB Design Goal: 0.4 pCi/ml (drinking water standard [3])

## Activation of soil and ground water

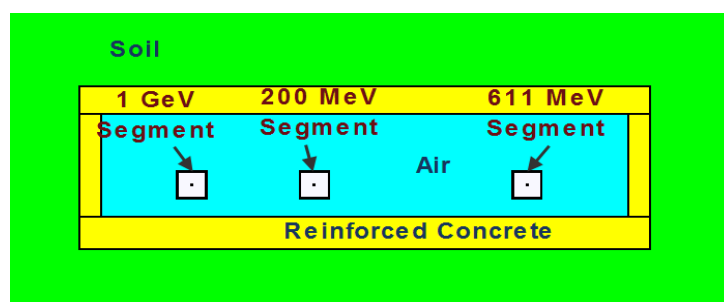
Some activation of the soil and the ground water is expected at the FRIB linac due to normal beam losses. Whereas the actual beam losses will be determined during facility operation, the design requirement for the linac is to keep it below 1 W/m. The level of activation was evaluated for an assumed beam loss rate of 1 W/m and radiologically bounding beam of protons at 200 MeV in the first linac segment (see Figure 1), 611 MeV in the second segment, and 1 GeV in the third segment. The calculations were carried out in two steps. As the first step, the star density distribution was calculated around the linac tunnel using the radiation transport code MARS15 [4-6]. The concentrations of dominant radionuclides  $^3\text{H}$  and  $^{22}\text{Na}$  were estimated from the star density using Radionuclide Concentration Model [7] after that.

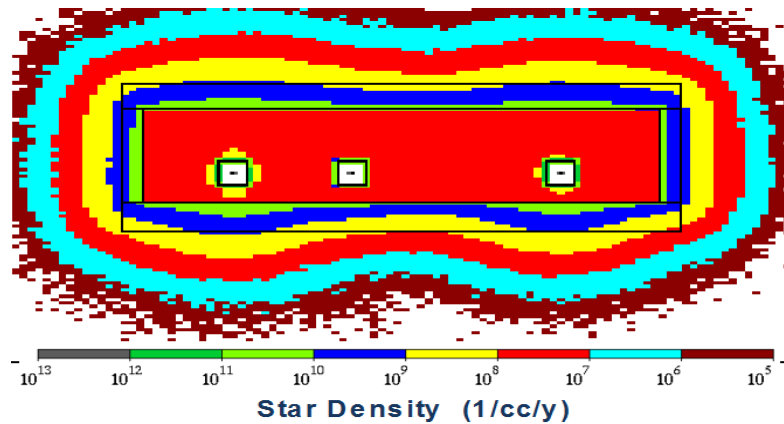
### Star density distribution due to normal beam losses

Figure 2 shows a cross-section of the double-folded FRIB linac, the tunnel walls and the surrounding soil. The associated proton beam energies are also indicated in the figure. Fermilab-type wet dirt [6] with a density of  $2.24 \text{ g/cm}^3$  was used as the soil (standard MARS15 material "SOIL"). The tunnel wall thickness used in the calculations was 30 in, and that of the tunnel roof is 42 in. The linac segments were represented with a stainless steel pipe surrounded with a box as cryogenic modules. The angle at which the beam particles entered the beam pipe material was set to 3 mrad with respect to the beam pipe surface, and the entry position is uniformly distributed both longitudinally and azimuthally. These assumptions are a simplification. In reality, a broader angular spectrum is possible, with the beam loss rate higher in focusing elements where the beam size is larger. The effect of the incident angle on the ground water activation was tested for angles 0.1 mrad, 3 mrad and 1 degree and no significant difference was found.

The resulting star density distribution with contribution from beam losses in all the segments is shown in Figure 3. The distribution is presented in units of  $1/\text{cm}^3/\text{y}$  assuming that one operational year is  $2 \times 10^7 \text{ s}$  (5556 h). It is recognised that a gradient in activity will be present from the edge of the facility. The soil and groundwater activation is assessed by assuming uniform mixing of the activated water over the assumed analysis volume. Activated soil and groundwater next to the tunnel wall poses no risk to the environment or the public. It must flow from this location to the "facility boundary" or "point of compliance" for the facility as described in the regulations. Therefore, the region can be assumed to effectively mix. The mixing of the water is taken into account by assessing the average star density over a volume that contains either 99% or 99.9% of the entire radioactivity generated in the soil. The 99% and 99.9% volumes were found to be restricted by isocontours located approximately 2 m and 3 m respectively from the concrete walls of the tunnel. These distances of 2 m and 3 m are measured against the segment 2 (611 MeV) and segment 3 (1 GeV) which are locations where the soil activity is maximum. In other places these isocontours are located even closer to the tunnel walls. The averaged star densities are summarised in Table 2.

**Figure 2. Cross-section of linac model with surrounding soil and tunnel walls**



**Figure 3. Resulting star density distribution****Table 2. Averaged star densities and limiting isocontour levels corresponding to 99% and 99.9% volumes**

Volume	Averaged star density [1/cm <sup>3</sup> /y]	Isocontour level [1/cm <sup>3</sup> /y]
99%	$2.99 \times 10^8$	$1.13 \times 10^7$
99.9%	$1.87 \times 10^8$	$1.24 \times 10^6$

The isocontours levels can be used to determine “points of compliance” from Figure 3.

### Nuclide concentrations

The averaged star densities are converted in radionuclide concentration using Radionuclide Concentration Model [7]. In the original model, the concentration  $C_i$  (in pCi per ml) for a radionuclide of the type  $i$  in water in proximity to the beam enclosure is expressed by:

$$C_i(t) = N_p \cdot S_{\max} \cdot G \cdot K_i \cdot L_i \cdot (1.17 \times 10^6 \cdot \rho \cdot w_i)^{-1} (1 - e^{-\lambda t}) \quad (1)$$

or, in the limit of radionuclide saturation, by:

$$C_i(t = \infty) = N_p \cdot S_{\max} \cdot G \cdot K_i \cdot L_i \cdot (1.17 \times 10^6 \cdot \rho \cdot w_i)^{-1} \quad (2)$$

where:

- $N_p$  is the number of incident protons per year;
- $S_{\max}$  is the maximum star density (in 1/cm<sup>3</sup>) per incident proton in the soil or rock obtained from calculations carried out with radiation transport codes;
- $G$  is the geometry factor which takes into account mixing of the activated water in some volume;
- $K_i$  is the radionuclide production probability per star (0.075 atoms/star for <sup>3</sup>H, 0.02 atoms/star for <sup>22</sup>Na in the original model, calculated in simulations in our case and presented in Table 3);
- $L_i$  is the leachability factor for the radionuclide (0.9 for <sup>3</sup>H and 0.135 for <sup>22</sup>Na in soil);
- $\rho$  is the material density;

- $w_i$  is the weight of water divided by the weight of soil needed to leach 90% of the leachable radioactivity that is present (0.27 for  $^3\text{H}$  and 0.52 for  $^{22}\text{Na}$ );
- $\lambda_i$  is the inverse mean lifetime of the radionuclide of the type  $i$ , measured in units consistent with those of time  $t$  (e.g. years);
- $1.17 \times 10^6$  is the numerical factor that converts disintegrations per second into  $p\text{Ci}$  (0.037) and years into seconds ( $3.15 \times 10^7$ ).

The averaging of the activated water is taken into account by the geometry factor,  $G$ . A typical value of  $G$  found in the literature is 0.19 for beam lines and 0.019 for target stations not followed by long beam lines [8]. The factor was analytically calculated as a ratio of the star density averaged out to a radius where the star density has fallen to 1% of its peak value over the peak star density. The calculations were performed for a system with a certain cylindrical symmetry. Sometimes this approach is erroneously called a “99% volume” approach assuming that in these calculations 99% of all the activation is contained in the volume over which this procedure is performed. This is only approximately correct, especially for systems where there is no cylindrical symmetry. In the present calculations, however, we do not rely on the knowledge of the geometry factor. The previously calculated averaged star density is used as described above. This changes Equations (1) and (2) to:

$$C_i(t) = N_p \cdot S_{aver} \cdot K_i \cdot L_i \cdot (1.17 \times 10^6 \cdot \rho \cdot w_i)^{-1} (1 - e^{-\lambda_i t}) \quad (3)$$

or in the limit of radionuclide saturation

$$C_i(t = \infty) = N_p \cdot S_{aver} \cdot K_i \cdot L_i \cdot (1.17 \times 10^6 \cdot \rho \cdot w_i)^{-1} \quad (4)$$

In these equations,  $S_{aver}$  is the star density averaged over volumes containing either 99% or 99.9% of all the activity, and is  $S_{max} \times G$ . The rates of radionuclide production per star,  $K_i$ , are also calculated. We do not rely on the values originally presented in the radionuclide concentration model. The number of lost particles  $N_p$  is energy dependent and is calculated assuming a beam loss rate of 1 W/m.

As discussed in [7] and [9], only two radionuclides  $^{22}\text{Na}$  and  $^3\text{H}$  are of importance for FNAL soil types based upon the production rates, half-life time and the leachability by water. The leaching factor,  $L_i$ , is probably the most uncertain parameter of the model. It is a fraction of radionuclides that can be washed out by a representative amount of water. As discussed in [9], measurements were made of the number of radionuclides washed out of a sample of material exposed to a known amount of beam, by successive mixings of known amounts of water. For  $^{22}\text{Na}$ , the amount washed out with each batch of water can be totalled and compared to the amount of activity initially present. This is not possible with the  $^3\text{H}$  leaching measurements, due to the low energy of its beta decay and the analytical techniques employed. Only a product of the leachability and radionuclide production probability per star,  $K_i$ , can be measured for tritium.

The concentration model chooses to use the quantity of water that removes 90% of the leachable radionuclides, and uses this amount of the water as the basis for conversion from the soil density,  $\rho$ , to the density of water in the soil, ( $\rho w_i$ ). The leachability for tritium in soil is 0.9, and has the meaning that the volume of water considered removes 90% of the amount of tritium that could be removed by continuing the washes to the necessary limit.

Table 3 summarises some parameters for the dominant radionuclides.  $K$ -factors were obtained from the simulations. Tables 4 and 5 show dominant radionuclide concentrations averaged over different volumes. The concentrations were calculated for three irradiation times: 10 years, 20 years and an infinite irradiation time (“saturation”). Beside the concentrations, the values  $\Sigma_i C_i / C_{i,max}$  are also shown. The values are the sums of concentrations of all radionuclides of importance divided by maximum allowed concentrations in drinking water. The regulatory requirements stipulate that the value

$\sum_i C_i/C_{i,max}$  must be less or equal to 1. The values of  $C_{i,max}$  for drinking water are found in [3] and also summarised in Table 3. As the calculations for the considered model showed, the radionuclide concentrations calculated in the 99.9% volume are expected to stay below the regulatory limits for drinking water standards for all radionuclides of importance both separately and in sum. These calculations are conservative for a number of reasons. The thickness of the tunnel walls has been increased from 30 in to 36 in after these calculations were completed; ion beams will be used instead of radiologically bounding proton beams in the baseline configuration of the facility, and heavier beams are expected to produce even less activity in the ground water; and in addition to that, we do not expect that the saturation conditions will even be achieved due to the seasonal variations of the water table.

**Table 3. Dominant radionuclide parameters and regulatory limits  $C_{max}$**

Nuclide	Half-life [y]	$C_{max}$ [pCi/ml]	Atoms per Star (K-factor)
$^3\text{H}$	12.32	20	0.0250
$^{22}\text{Na}$	2.6027	0.4	0.00732

**Table 4. Concentrations of radionuclides averaged over the volume containing 99% of activity**

Irradiation 10 years			Irradiation 20 years			Saturation		
$C(^3\text{H})$ [pCi/ml]	$C(^{22}\text{Na})$ [pCi/ml]	$\sum_i C_i/C_{i,max}$	$C(^3\text{H})$ [pCi/ml]	$C(^{22}\text{Na})$ [pCi/ml]	$\sum_i C_i/C_{i,max}$	$C(^3\text{H})$ [pCi/ml]	$C(^{22}\text{Na})$ [pCi/ml]	$\sum_i C_i/C_{i,max}$
4.10	0.20	0.71	6.44	0.22	0.86	9.54	0.22	1.02

**Table 5. Concentrations of radionuclides averaged over the volume containing 99.9% of activity**

Irradiation 10 years			Irradiation 20 years			Saturation		
$C(^3\text{H})$ [pCi/ml]	$C(^{22}\text{Na})$ [pCi/ml]	$\sum_i C_i/C_{i,max}$	$C(^3\text{H})$ [pCi/ml]	$C(^{22}\text{Na})$ [pCi/ml]	$\sum_i C_i/C_{i,max}$	$C(^3\text{H})$ [pCi/ml]	$C(^{22}\text{Na})$ [pCi/ml]	$\sum_i C_i/C_{i,max}$
2.56	0.13	0.44	4.02	0.13	0.54	5.95	0.14	0.64

### Comparison of FNAL and FRIB soil

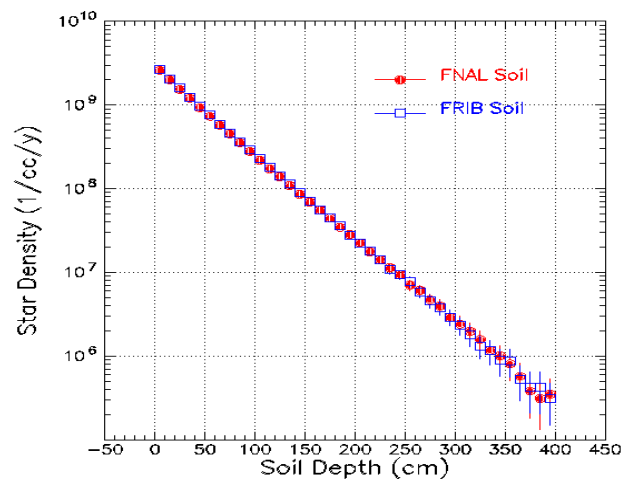
Although the evaluation of the soil and ground water activation was performed using FNAL-type soil, a comparison between this type of soil and actual FRIB soil was also carried out. NTH Consultants, Ltd. [10] performed a geological survey taking a number of samples at various locations and depths (up to 75 ft) on the FRIB site. The moisture content and the element composition were determined. It was found that although the soil composition varies from sample to sample, the averaged composition and the density is somewhat similar to those of the FNAL-type soil. The soil compositions are compared in Table 6. The averaged density of the FRIB soil was found to be 2.257 g/cm<sup>3</sup> versus that of 2.24 g/cm<sup>3</sup> for the FNAL soil. To further validate the similarity, Monte Carlo calculations were conducted using a simple cylindrically symmetrical model with dimensions that resemble those found in the actual FRIB tunnel. Star density was calculated for both soil types. A beam of 1 GeV protons was used.

Figure 4 shows two star density distributions as a function of soil depth for both types of soil. Both distributions are similar which validates that the results previously obtained with the FNAL-type wet dirt are applicable to the FRIB site.

**Table 6. Composition of averaged FRIB soil and FNAL-type wet dirt**

Element	Z	A	Weight fraction (FNAL)	Weight fraction (FRIB)	Atomic fraction (FNAL)	Atomic fraction (FRIB)
H	1	1.00794	0.023	0.016	0.31	0.23
C	6	12.01100		0.028		0.035
O	8	15.99940	0.57	0.61	0.49	0.56
Mg	12	24.30500		0.020		0.012
Al	13	26.98154	0.071	0.034	0.036	0.018
Si	14	28.08550	0.33	0.21	0.16	0.11
K	19	39.09830		0.0094		0.0036
Ca	20	40.07800		0.060		0.022
Ti	22	47.88000		0.0022		0.00069
Fe	26	55.84500		0.014		0.0038

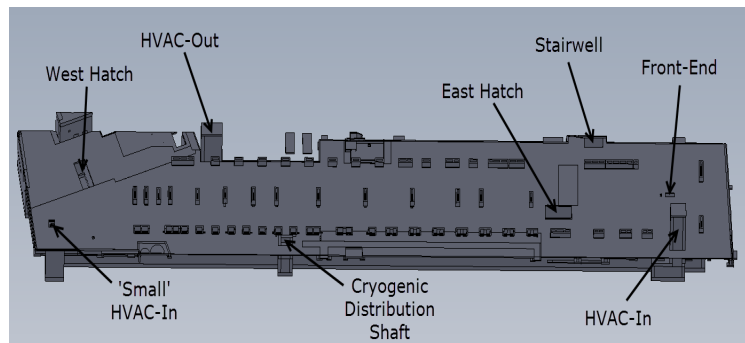
**Figure 4. Star density distribution as a function of the soil depth**



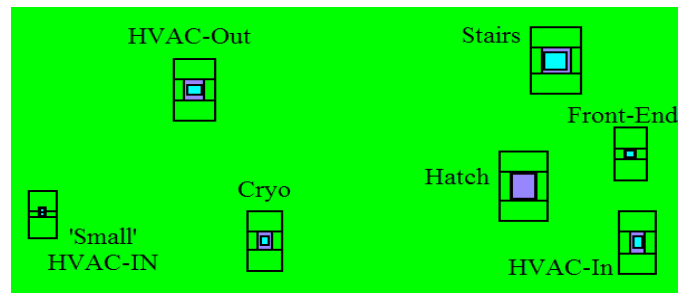
### Effect of major penetrations

The linac tunnel will be located approximately 6 m under the surface. This shielding of 6 metres (concrete and soil) is not solid, however. There is a number of small penetrations through the shielding like those for radio-frequency wave guides, cables and services, and several big penetrations. These major penetrations (see Figure 5) are the front-end drop; heating, ventilation and air conditioning inlet (HVAC-In); second (smaller) HVAC inlet ("Small" HVAC-In); HVAC outlet (HVAC-Out); hatch on the east side of the linac tunnel (East Hatch); stairwell on the north-east side of the linac tunnel; and cryogenic distribution shaft (Cryoline). Due to their substantial size, one expects an enhanced radiation streaming through them which, in turn, will increase the level of the soil and ground water activation. An effect of the major penetrations on the ground water activation was studied in two sets of calculations. The star densities were calculated in volumes surrounding these penetrations (see Figure 6). The volume size was chosen to be 3 m which approximately corresponds to the 99.9% volume as described in the previous sections. The star densities were compared to values obtained in the second set of calculations using the same model but with the major penetrations removed (Figure 7). The direct comparison between the two sets of star density values allows us to estimate the effect of the penetrations on the ground water activation. The calculations were performed for a constant beam loss of 1 W/m for radiologically bounding beams: protons at 611 MeV in the second linac segment and the second folding segment, and protons at 1 GeV in the third linac segment. The beam losses in the first linac segment and the first folding segment were ignored due to the fact that these segments would not be used for the proton beams, and that the energy of other ion beams in this segment will be as low as 20 MeV/nucleon or below. Table 7 provides the comparison between those two sets of star density values for each of the major penetrations. One can see that the values are less than 33% different. Thus the conclusions of our previous studies are not affected.

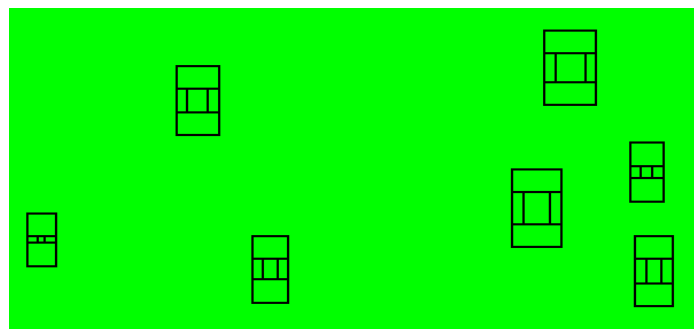
**Figure 5. Three-dimensional rendering of the concrete structure of the linac tunnel and the service building**



The area above the surface level is clearly seen. The major penetrations are indicated.

**Figure 6. Plan view of model above the tunnel**

Volumes around the penetrations in which the star densities were calculated are shown.

**Figure 7. Plan view of model above the tunnel**

Volumes around the penetrations in which the star densities were calculated are shown. The model is similar to that shown in Figure 6, but the major penetrations were removed from it.

**Table 7. Averaged star densities calculated in 3 m-thick volumes located around the major penetrations**

Penetration	Averaged star density in model with major penetrations [1/cm <sup>3</sup> /y]	Averaged star density in model with major penetrations removed [1/cm <sup>3</sup> /y]	Star density increase due to penetration [%]
Front end	8.79E+07	8.15E+07	7.3
HVAC-In	4.52E+07	3.99E+07	11.7
East Hatch	1.89E+08	1.27E+08	32.5
Cryoline	6.68E+07	5.92E+07	11.3
Stairs	2.35E+06	1.87E+06	20.2
HVAC-Out	8.95E+07	7.76E+07	13.3
'Small' HVAC-In	5.83E+06	5.61E+06	3.8

Also shown are the averaged star densities calculated in the same volumes but in the model where the penetrations were removed.

### **Prompt dose rates**

As part of the design process, we need to ensure that the facility provides an adequate shielding so that the dose equivalent rates stay below the MSU ALARA goals for both the workers and the general public. In the case of prompt dose radiation at the FRIB linear accelerator, the limits apply to the areas above the surface (grade) only, because the machine was not designed to allow access into the beam enclosure during the operation. It is important to note that the facility is located on the MSU campus, and that the members of the general public can be present close to the facility walls. The dose rates must be evaluated for both the normal operation (1 W/m beam loss rate) and beam loss incident scenarios, and compared to both the personnel and general public dose limits. All the calculations for this purpose were performed with the MARS15 code [4-6] using a model that includes the linear accelerator, tunnel, all major penetrations and other conduits, and the walls of the service building above grade.

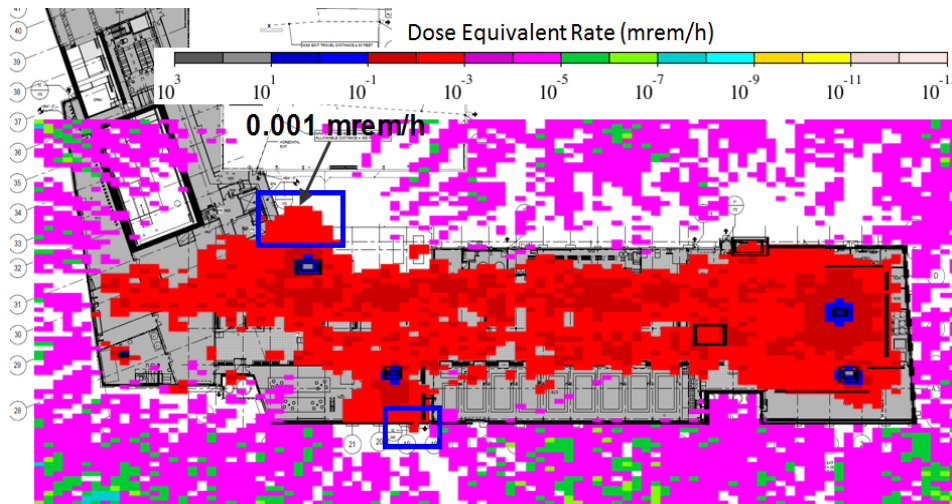
#### **Prompt dose rates during normal operation**

MSU ALARA stipulates that the annual doses should not exceed 500 mrem for the workers, and 10 mrem for members of the general public. These numbers translate into 0.25 mrem/h and 0.0018 mrem/h ALARA goals assuming that one working year during which the exposure of the workers to the radiation is possible is 2000 hours, and one operational year during which the general public can be exposed to is 5556 hours. We do not claim any credit for the general public to be around FRIB for only part of the year.

The dose equivalent rate above grade was calculated for the radiologically bounding beams: protons at 611 MeV in the second linac segment and the second folding segment, and protons at 1 GeV in the third linac segment. In addition, we added the beam losses for <sup>18</sup>O beam at 35 MeV/nucleon in the first linac segment and the first folding segment. These segments would not be used for protons. The resulting dose rate distribution is shown in Figure 8. The distribution is overlaid with a plan view of the facility. A number of recommendations were made based on this distribution for the purpose of protection of the general public: the walls of the service building constructed with CMU blocks should be filled with grout in several locations (see Figure 9); the fence on the north side of the building should be realigned to restrict access of the general public to that area; and the shielding above the surface for the cryogenic distribution shaft must be redesigned.

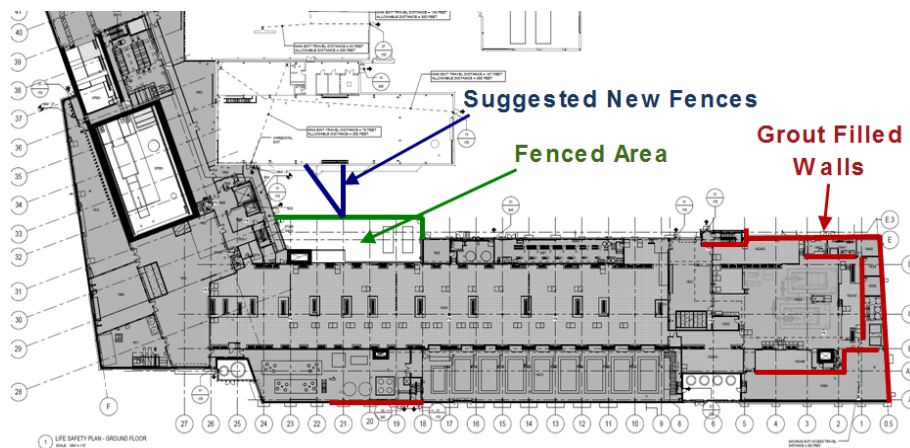
The dose map also confirmed that the dose rate is below 0.1 mrem/h everywhere in the service building with exception of the vicinity of the major penetrations. The dose rate of 0.1 mrem/h is in fact the MSU ALARA goal for the workers with additional safety margin of 2.5. A closer look at the dose rate around the major penetrations revealed that it is only a small numerical factor higher than 0.1 mrem/h and in relatively small areas with size in a scale of a meter. A number of mitigation strategies can be applied in these areas such as active monitoring, local shielding that would not impact the operation, stand-offs, and occupancy factors in locations where the workers are not expected to be during the entirety of their shift. Other penetrations such as conduits for radio-frequency wave guides appear to be small enough and well shielded to keep the dose rates in their vicinity below 0.1 mrem/h.

**Figure 8. Dose equivalent rate distribution calculated above grade and expressed in units of mrem/h**



The blue boxes indicate publically accessible areas where the dose rate exceeds 0.001 mrem/h.

**Figure 9. Plan view of the service building at the grade level**



The red lines indicate building walls that are suggested to be filled in with grout. The green lines limit an area outside the service building that is planned to be fenced out. The blue lines show fence locations which will limit the public access to the area because the expected dose rate will exceed 0.001 mrem/h.

### **Prompt dose rates due to beam loss incidents**

The dose equivalent rates in the service building above grade due to beam loss incidents were also evaluated. Radiologically bounding proton beams were used. We also assumed that the beam is completely stopped in a stopping target. This is rarely the case, however. Particle beams are not normally lost locally but rather on a stretch of accelerator because an actual beam has a size and particles in the beam have angular distribution. And, if the beam is lost due to a magnet failure, the field in the magnet changes slow enough to spread the beam losses over a section of the machine. Therefore, the assumption of the local beam losses will result in conservative estimates. The positions of the stopping target were selected to maximise to dose rates around the major penetrations, since the dose rate increase due to smaller conduits is not substantial. The intensity of the stopped

beam was  $2.5 \times 10^{15}$  1/s, which corresponds to 400 kW of 1 GeV protons (beam power on the production target). It was found that the maximum dose rate reaches  $1.8 \times 10^4$  mrem/h. This dose rate is found at the front-end drop when the beam is lost in one of the locations in the second folding segment. The MSU ALARA stipulates that the dose rate stays below 2 mrem in any one hour for the workers. The limit of 2 mrem in any one hour is also a regulatory limit for the general public. Further assuming that the accelerator will be shut down after such an incident to investigate the reasons for the lost beam and therefore no more than one beam loss incident in any one hour is possible, we will need to detect such beam loss event and shut down the machine in 0.4 s. Note that the machine protection system is being designed to do so in just 35  $\mu$ s. Therefore the beam loss incidents should not pose a risk to people from the standpoint of the prompt dose.

### **Activation of water services**

There are several thousand gallons of water in two closed-loop systems at the FRIB linac. The LCA system (Low Conductivity Activated) will hold  $\approx 6435$  gallons to cool various beam line elements and magnets. Approximately, 1425 gallons in the CHA system (Chilled Activated) will be used for the HVAC units in the tunnel. Both systems will have an extensive plumbing and various purpose tanks in the linac tunnel and the service building above grade. Since this water is directly exposed to the radiation from the linac, we need to know both radionuclide concentrations and the total amount of radioactivity produced in these systems. These values are used in spill analyses of the activated water and in calculations of the doses to the workers from the activated water contained in the plumbing.

### **Radionuclide inventories in LCA and CHA systems**

The dominant radionuclides produced in water in the accelerator environment are  $^3\text{H}$  (tritium),  $^7\text{Be}$ ,  $^{11}\text{C}$ ,  $^{13}\text{N}$  and  $^{15}\text{O}$  [12]. These radionuclides are produced via spallation reactions induced by nucleons with the energy above 20 MeV. Fluxes of such nucleons were calculated in the LCA and CHA systems with MARS15 [4-6] for the normal beam losses (1 W/m) and the radiologically bounding proton beam. The fluxes were then converted into concentrations of the radionuclides of importance using a model described in [12]. The concentrations were calculated for broad ranges of the irradiation time (from 1 month to saturation) and the cooling time (from 0 to 1 year). The activities produced by ion beams at the same beam loss rate of 1 W/m are expected to be lower. The total activities were also calculated since the volumes of water directly exposed to the radiation in both systems are known. Both activities per unit volume and the total activities in the case of unlimited irradiation (saturation) and no cooling time allowed are summarised in Table 8. This case is the worst case scenario. The activities will decrease if a cooling time is assumed. For accident scenarios involving spills or leaks, the saturation case with no decay time should be used.

**Table 8. Activities per unit volume and total activities of dominant radionuclides produced in water in the LCA and CHA systems for unlimited irradiation time (saturation) and no cooling time allowed**

Radionuclide	LCA		CHA	
	Activity per unit volume [ $\mu\text{Ci/ml}$ ]	Total activity [ $\mu\text{Ci}$ ]	Activity per unit volume [ $\mu\text{Ci/ml}$ ]	Total activity [ $\mu\text{Ci}$ ]
$^3\text{H}$	1.53E-02	3.73E+05	1.59E-03	8.57E+03
$^7\text{Be}$	2.55E-03	6.21E+04	2.65E-04	1.43E+03
$^{11}\text{C}$	3.57E-04	8.70E+03	3.71E-05	2.00E+02
$^{13}\text{N}$	4.59E-03	1.12E+05	4.77E-04	2.57E+03
$^{15}\text{O}$	2.04E-02	4.97E+05	2.12E-03	1.14E+04

### Dose rates at LCA and CHA systems

A further analysis allows calculations of the dose rates at the various components of the LCA and CHA systems using the estimated radionuclide concentrations. This was carried out with the code MicroShield6 [13]. Both the LCA and CHA systems have four types of cylindrically shaped tanks. These are air separators (Gas Liquid Separators, GLS), carbon filter tanks, ion exchangers (DI), and expansion tanks. There are two tanks of each type in each system. The tanks are located in a designated room in the service building. The tanks are not completely filled with activated water and have components inside which provide additional shielding against photons emitted from decaying radionuclides in water. In our calculations we assume that the tanks are filled with the water entirely. Thus, our calculations are conservative. There are also three heat exchangers in the LCA system and two in the CHA system, and regular pipes.

We assumed that a possible build-up of  $^7\text{Be}$  anywhere in the LCA and CHA systems is insignificant and can be ignored. The build-up might occur due to  $^7\text{Be}$  ions attaching to the plumbing if the water dynamics allows it. There are two factors, however, that suggest the low level of the build-up. First, the ions of  $^7\text{Be}$  will be continuously removed from the systems by the ion exchange columns with efficiency of approximately 95% per cycle. Second, our collaborators from Spallation Neutron Source (SNS) reported that the build-up of  $^7\text{Be}$  in their similar systems was insignificant. The dose rates were calculated, however, assuming that no  $^7\text{Be}$  is removed from the LCA and CHA systems. Thus our calculations are conservative.

The dose equivalent rates at various components of the LCA and CHA systems are summarised in Tables 9 and 10. The dose rates were calculated at a distance of one foot from the components, assuming that the water in the system was irradiated for an infinite amount of time (saturation). The calculations were carried out for a moment immediately after the beam shut-down (0 hour delay), and 4 hours after the beam shut-down. We also assumed that no radionuclides are removed from water by any filters. The dose rates were calculated in two locations for each cylindrical tank assuming that these tanks are placed vertically: one foot from the cylindrical surface in the middle plane of the tank ("Side" in the tables); and one foot from the flat surface of the tanks ("Top" in the tables). Similarly, the dose rates were calculated in two locations for the heat exchangers: one foot from the middle point of the side surface ("Side" in the tables, the largest surface of the heat exchangers); and one foot from the middle point of the front or end surface ("Face" in the tables). Generally, the dose rates at the LCA components are more than an order of magnitude higher than those at the CHA components. The highest dose rate is

observed on the sides of the heat exchangers due to their significant size and small amount of shielding.

The contributions to the dose rates with no decay time allowed come mostly from short-lived nuclides  $^{11}\text{C}$ ,  $^{13}\text{N}$ , and  $^{15}\text{O}$ . Letting the radionuclide decay for 4 hours reduces the dose rates by more than two orders of magnitude, and  $^3\text{H}$  and  $^7\text{Be}$  become the dominant nuclides. However, as long as tritium remains contained by the plumbing, only  $^7\text{Be}$  will be contributing to the dose rate outside the plumbing due to a low energy of electrons produced in the tritium decay.

**Table 9. Dose equivalent rates (mrem/h) at a one foot distance from various components of the LCA system**

– Tank/Device	– Side		– Top (“Face” for Heat Exchanger)	
	– 0 hours decay	– 4 hours decay	– 0 hours decay	– 4 hours decay
– Air Separator/GLS	– 4.801	– 2.373E-02	– 3.228	– 1.596E-02
– Heat Exchanger	– 2.307E+01	– 1.139E-01	– 2.918E-01	– 1.306E-03
– Expansion Tank	– 5.657	– 2.793E-02	– 4.320	– 2.135E-02
– DI	– 7.829	– 3.856E-02	– 7.605	– 3.756E-02
– Carbon Filter	– 7.829	– 3.856E-02	– 7.605	– 3.756E-02
– Pipe in Tunnel	– 2.190	– 1.086E-02	–	–

**Table 10. Dose equivalent rates (mrem/h) at a one foot distance from various components of the CHA system**

– Tank/Device	– Side		– Top (‘Face’ for Heat Exchanger)	
	– 0 hours decay	– 4 hours decay	– 0 hours decay	– 4 hours decay
– Air Separator/GLS	– 3.038E-01	– 1.506E-03	– 1.806E-01	– 8.898E-04
– Heat Exchanger	– 1.861	– 9.169E-03	– 3.121E-02	– 1.392E-04
– Expansion Tank	– 2.934E-01	– 1.449E-03	– 1.805E-01	– 8.894E-04
– DI	– 3.515E-01	– 1.735E-03	– 1.808E-01	– 8.904E-04
– Carbon Filter	– 3.515E-01	– 1.735E-03	– 1.808E-01	– 8.904E-04
– Pipe in Tunnel	– 7.780E-02	– 3.845E-04	–	–

### Low-level liquid waste

There will be two more sets of tanks in the service building for Low Level Liquid Waste (LLLW). One set will store low-level activity water that is assumed to be condensed and collected on the HVAC cooling coils in the tunnel. The other set is for the condensed water from the tunnel walls and the magnets. Unlike the tanks in the two closed-loop systems, the LLLW tanks release activated vapour (humidity above the free surface) when additional water is added to the tanks and is released through the SMOG system to the environment. The activated water collected in LLLW will be removed as the tanks get filled, releasing the activated water vapour that has had a chance to decay in the LLLW tank. It was estimated that in the worst case mode as much as 9400 gallons of condensed water can be collected from the HVAC units in a full year operation. This mode of operation is unlikely, however, in the controlled climate of the facility.

Two sources of radionuclides in LLLW are possible: a direct production in water that has been already condensed, and production of the nuclides in the tunnel air with their

consequent capture by the water condensate. The concentrations of the nuclides produced by the first mechanism were calculated using the same approach as used for water in the LCA and CHA systems. Similar model was also used for the production of  $^3\text{H}$ ,  $^7\text{Be}$ ,  $^{11}\text{C}$ ,  $^{13}\text{N}$  and  $^{15}\text{O}$  in the tunnel air via spallation reactions caused by the nucleons with the energy above 20 MeV. A yield of  $^{41}\text{Ar}$  in air was estimated directly by taking into account a capture of thermal neutrons. All the nuclide concentrations were found to be quite low, and thus this low-activated water can be processed with the existing MSU systems.

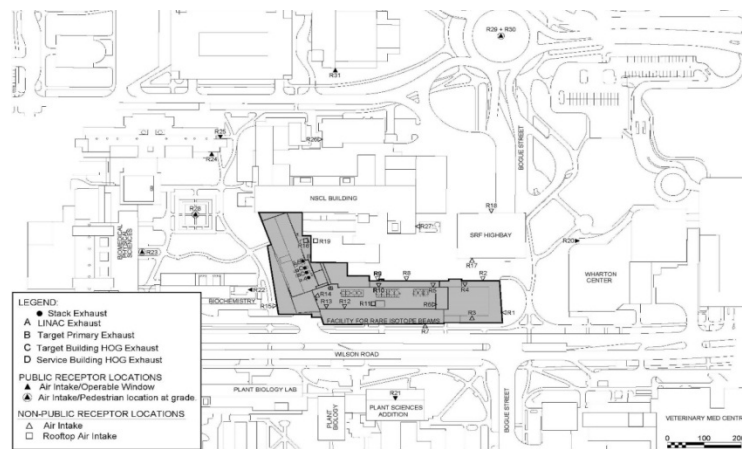
### **Independently validated design basis air effluent**

FRIB operation inherently activates air in the linac tunnel and the target building hot cell. Additionally gaseous releases associated with activated water in the facility result in normal operational effluent from the facility. This effluent is filtered with both activated charcoal and HEPA filters to remove a significant portion of the activated material from the gaseous effluent. This effluent is released to the environment through high velocity exhaust stacks on the top of the FRIB target building. The potential impact on the public from these releases must be conservatively evaluated to assure that regulatory release limits and ALARA goals (Table 1) can be met during operation. Actual exposure will be determined by monitoring and is anticipated to be significantly lower than these conservatively estimated releases.

Airborne consequence analysis was performed in two steps. First, the various sources of air activation and gaseous activated products were determined from radiation transport calculations. These included the tunnel air HVAC exhaust and hot cell air HVAC exhaust, as well as the gaseous releases from activated systems from the target facility hot off-gas system (HOG) and service building special mechanical off-gas system (SMOG). These sources were then evaluated for potential public consequence based on both decay and dispersion from the stack [11]. A key factor in this evaluation is the potential wind conditions at FRIB accounting for the normal annual variations in wind, the impact of surrounding buildings, and the potential location of public receptors. This evaluation was performed using scale model wind tunnel testing (Figure 10) and the local historical wind data for this area. An appropriate set of receptor locations were identified to provide a representative sample of receptor location (Figure 11). The results of the evaluation accounting for the conservative source term, radioactive decay in the time to reach the receptors, and dispersion as defined by the wind tunnel data show that the regulatory limits and MSU ALARA goals can be easily met.

**Figure 10. Wind tunnel scale model**



**Figure 11. Receptor locations evaluated**

## Conclusions

This paper provides an overview of the range of conservative radiation transport analyses performed in support of the FRIB design. The focus is on analyses that demonstrate compliance with NRC limits and MSU ALARA goals for postulated human and environmental exposure. Actual exposure will be based on measurements during commissioning and operation. These radiation calculations demonstrate anticipated acceptability and support the start of technical construction. Radiation transport will continue to support the designers, to ensure the completion of the final design, commissioning and operations.

## Acknowledgements

This material is based on work supported by the US Department of Energy Office of Science under Cooperative Agreement DE-SC0000661.

## References

- [1] Standards for sump water, Nuclear Regulatory Commission, 10 CFR 20.
- [2] MSU ALARA – NRC License Number 21-00021-29, MSU Type A Broad Scope License. MSU operates as a fully-licensed, non fuel cycle R&D Type A, NRC broad-scope licensee since 1977.
- [3] Standards for drinking water, Environmental Protection Agency, 40 CFR 141.
- [4] N.V. Mokhov (1995), "The Mars Code System User's Guide", Fermilab-FN-628.
- [5] N.V. Mokhov, S.I. Striganov (2007), "MARS15 Overview", Fermilab-Conf-07/008-AD; *Proc. of Hadronic Shower Simulation Workshop*, Fermilab, September 2006, AIP Conf. Proc. 896, pp. 50-60.
- [6] <http://www-ap.fnal.gov/MARS/>.
- [7] A. Wehmann, W. Smart, S. Menary, J. Hylen and S. Childress (1997), "Groundwater Protection for the NuMI Project", FERMI LAB-TM-2009.
- [8] Bill Freeman (1996), "A NuMI Wide-Band Beam Shield Design That Meets the Concentration Model Groundwater Criteria", NuMI Note B-155.

- [9] A.J. Malensek, A.A. Wehmann, A.J. Elwyn, K.J. Moss and P.M. Kesich (1993), "Groundwater Migration of Radionuclides at Fermilab", FERMILAB-TM-1851.
- [10] NTH Consultants, Ltd.; <http://www.nthconsultants.com/>.
- [11] RWDI; <http://www.rwdi.com/>.
- [12] J.D. Cossairt (2000), "Calculation of the Radioactivity Produced in the Cooling Loops of the CDF SVX II Detector", Fermilab-TM-2112.
- [13] MicroShield6 code; <http://www.radiationsoftware.com/>.